ISSN 2072-0149

The AUST

JOURNAL OF SCIENCE AND TECHNOLOGY

Volume-I Issue-I January 2009

Ahsanullah University of Science and Technology

THE AUST
Journal of Science and Technology
Vol - I, Issue - I, January '09

Mixed Convection in a Vee-Corrugated Enclosure with Isoflux Heating from Below

Sumon Saha[1], Md. Quamrul Islam[2] and Goutam Saha[3]

ABSTRACT : A numerical investigation has been carried out for mixed convection flow inside an enclosure applying isoflux heating from bottom. Air is forced to flow inside the ventilated enclosure at uniform velocity and temperature. In this work we examined the effect of corrugation frequency and the buoyancy force parameter on the flow and heat transfer characteristics. The non-dimensional governing equations are solved by using Galerkin's finite element method. The Richardson number, Ri varies from 0.1 to 10, corrugation frequency, C.F. varies from 0 to 3 and Reynolds number, Re is taken as 100. The results indicate that the average heat transfer coefficient is highest for low corrugation frequency but the reverse trend is found for high corrugation frequency. Finally a correlation between the non-dimensional governing parameter has been developed within the given range of computations.

Key words: *Mixed convection, Open enclosure, Richardson number, Reynolds number, Vee-corrugated wall.*

1. INTRODUCTION

The contemporary advancement in semiconductor technology is to be miniaturized in circuit design, resulting dramatic increase in the amount of dissipated heat per unit volume of a device. Maintaining the desired operating temperature by forced convection and buoyancy effects, lead to a mixed convection situation. Richardson number gives a qualitative indication of the influence of buoyancy on forced convection. Mixed convection may offer the potential for significant cooling enhancement with only modest penalty in system pressure losses, and such flow condition may be well suited to electronics cooling. Under low forced conditions, with increase in heat fluxes within the device, the buoyancy effect assumes greater importance, leading to a mixed convection situation.

Buoyancy-driven flow and heat transfer in open-ended enclosures is receiving increasing attention by many researchers in recent years. Mixed convection in open-ended cavities has been the subject of interest both experimentally and numerically. This interest is dictated by the role played by such configurations in the field of the habitat, the design of the solar heat collectors and more recently the cooling of the electronic cards (because of the tendency to the miniaturization of the components). An exhaustive review of the literature shows that the case of mixed convection in a ventilated system was examined by several authors. Oosthuizen and Paul (1985) studied numerically using the Galerkin finite element method mixed convection heat transfer in a cavity with uniformly heated, isothermal vertical walls and horizontal adiabatic walls.

[1]*Department of Mechanical Engineering, The University of Melbourne, Australia*
[2]*Department of Mechanical Engineering, Bangladesh University of Engineering and Technology*
[3]*Department of Mathematics, University of Dhaka*

A similar study was conducted by Simoneau *et al.* (1988) on the interaction between an injection and laminar natural convection in a thermally driven cavity. A comprehensive study was conducted by Khanafer and Vafai (2000), Khanafer *et al.* (2002) and Manca *et al.* (2003) to investigate basic aspects and physics of the flow field within the open-ended structures and the effect of the extended computational domain on the flow and heat transfer inside the open domain and its immediate surroundings. Papanicolaou and Jaluria (1990, 1993) studied various aspects of the mixed convection flow in adiabatic vented enclosures with isolated thermal sources flush with the inner walls.

Flow and heat transfer from irregular surfaces are often encountered in many engineering applications to enhance heat transfer. Most of the previous studies on enclosures with a form of irregular surfaces were concerned with natural convection. Das and Mahmud (2003) conducted a numerical investigation of natural convection in an enclosed consisting of two isothermal horizontal wavy walls and two adiabatic vertical straight walls. Also, Adjlout *et al.* (2002) have studied laminar natural convection in an inclined cavity with a heated undulated wall, i.e. smooth wave-like pattern. Their results concluded that the hot wall undulation affects the flow and heat transfer rate in the enclosure in which the local Nusselt number distribution results in a decrease of heat transfer rate as compared with the square enclosure. Moreover, Kumar (2000) conducted a study of flow and thermal field inside a vertical wavy enclosure filled with a porous media. The author has illustrated that the surface temperature was very sensitive to the drifts in the surface undulations, phase of the wavy surface and the number of considered waves.

However, the effect of corrugated wall was often neglected in the majority of the available studies in spite of its significant contribution to the natural convection heat transfer in such systems. Its effect was rather taken into account in rectangular geometries by Ali and Husain (1992, 1993), Ali *et al.* (2001), Fabbri (2000) in the case of natural convection. Chinnappa (1970) carried out an experimental investigation on natural convection heat transfer from a horizontal lower hot vee-corrugated plate to an upper cold flat plate. He took data for a range of Grashof numbers from 10^4 to 10^6. The author noticed a change in the flow pattern at Gr = 8×10^4, which he concluded was a transition point from laminar to turbulent flow. Randall *et al.* (1979) studied local and average heat transfer coefficients for natural convection between a vee-corrugated plate (60° vee-angle) and a parallel flat plate to find the temperature distribution in the enclosed air space. The author recommended a correlation in which the heat flux was 10% higher than that for parallel flat plates.

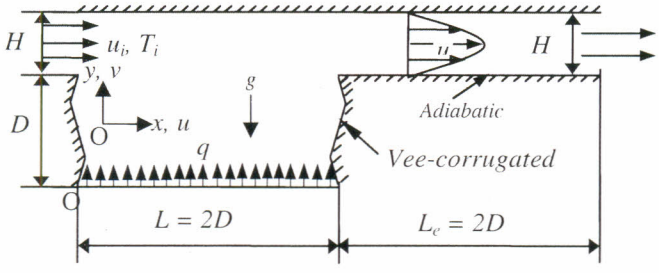

Fig. 1: Schematic Diagram of the physical model of Vee-corrugated cavity (C.F.=1)

In comparison with these studies, the case of open systems with corrugated vertical walls in mixed convection hardly starts to arouse interest and thus motivates us to perform the current investigation. Figure 1 shows the schematic diagram of the problem under consideration. It consists of an open cavity with vee-corrugated side walls of height D, width L (= 2D) and exit length L_e (= 2D). A Cartesian coordinate system is used with the origin at the lower left hand corner of the computational domain. The height of the inflow and outflow openings, *H* is taken half of the cavity height, *D* as examined from Manca *et al.* (2003) for obtaining maximum heat transfer rate. The corrugation amplitude has been fixed at 5% of the cavity height for all simulations, where the amplitude is defined as half of the horizontal distance measured from the left extremity of any side wall to its right extremity as shown in Fig. 1. However, for the fixed cavity height as well as constant corrugation amplitude, the vee-angle of the corrugated walls depends on the number of corrugation frequency (C.F.) of the side walls in the present problem. A uniform heat flux, q is applied to the bottom wall and the other walls are adiabatic. Flow enters through the left opening at a uniform mean velocity, u_i and temperature, T_i. The outgoing flow is assumed to have zero diffusion flux for all variables (outflow boundary conditions). The objective of this work consists in studying the effect of corrugation frequencies for mixed convection in a rectangular cavity, uniformly heated from below. The effect of the buoyancy parameter on the flow fields, the temperature distribution and the heat transfer rate are also investigated.

2. MATHEMATICAL EQUATIONS

The non-dimensional Navier-Stokes equations for two-dimensional, incompressible steady flow with constant properties except the Boussinesq approximation in Cartesian co-ordinates can be written as follows:

$$\frac{\partial U}{\partial X}+\frac{\partial V}{\partial Y}=0 \tag{1}$$

$$U\frac{\partial U}{\partial X}+V\frac{\partial U}{\partial Y}=-\frac{\partial P}{\partial X}+\frac{1}{Re}\left(\frac{\partial^2 U}{\partial X^2}+\frac{\partial^2 U}{\partial Y^2}\right) \tag{2}$$

$$U\frac{\partial V}{\partial X}+V\frac{\partial V}{\partial Y}=-\frac{\partial P}{\partial Y}+\frac{1}{Re}\left(\frac{\partial^2 V}{\partial X^2}+\frac{\partial^2 V}{\partial Y^2}\right)+Ri\,\theta \tag{3}$$

$$U\frac{\partial \theta}{\partial X}+V\frac{\partial \theta}{\partial Y}=\frac{1}{RePr}\left(\frac{\partial^2 \theta}{\partial X^2}+\frac{\partial^2 \theta}{\partial Y^2}\right) \tag{4}$$

Equations (1-4) were normalized using the following dimensionless scales:

$$X=\frac{x}{D},\ Y=\frac{y}{D},\ \theta=\frac{T-T_i}{(qD/k)} \tag{5}$$

$$U=\frac{u}{u_i},\ V=\frac{v}{u_i},\ P=\frac{p}{\rho u_i^2} \tag{6}$$

The Grashof number (*Gr*), the Prandtl number (*Pr*), the Reynolds number (*Re*), and the Richardson number (*Ri*) are given by

$$Gr=\frac{\beta g q D^4}{\upsilon^2 k},\ Pr=\frac{\upsilon}{\alpha},\ Re=\frac{u_i D}{\upsilon},\ Ri=\frac{Gr}{Re^2} \tag{7}$$

where α, β, ρ and υ are thermal diffusivity, thermal expansion coefficient, fluid density and kinematic viscosity respectively.

The average Nusselt number of the heated wall is calculated as

$$Nu = \frac{1}{L}\int_0^L \frac{h(x)x}{k}dx \tag{8}$$

where h is the local convective heat transfer coefficient and L is the length of the heated surface.

3. FINITE ELEMENT FORMULATION

The set of non-dimensional equations in terms of the stream function Ψ, the vorticity function Ω and the temperature θ are as follows:

The stream function Ψ is defined as

$$U = \frac{\partial \Psi}{\partial Y} \quad \text{and} \quad V = -\frac{\partial \psi}{\partial X}$$

And the vorticity function Ω is defined as

$$\Omega = -\left(\frac{\partial^2 \Psi}{\partial X^2} + \frac{\partial^2 \Psi}{\partial Y^2}\right)$$

Then Eqs. (1)-(4) becomes

$$\frac{\partial^2 \Psi}{\partial X \partial Y} - \frac{\partial^2 \Psi}{\partial X \partial Y} = 0 \tag{9}$$

$$\left(\frac{\partial \Psi}{\partial Y}\frac{\partial \Omega}{\partial X} - \frac{\partial \Psi}{\partial X}\frac{\partial \Omega}{\partial Y}\right) = \frac{1}{\mathrm{Re}}\left(\frac{\partial^2 \Omega}{\partial X^2} + \frac{\partial^2 \Omega}{\partial Y^2}\right) + \mathrm{Ri}\left(\frac{\partial \theta}{\partial X}\right) \tag{10}$$

$$\frac{\partial \Psi}{\partial Y}\frac{\partial \theta}{\partial X} - \frac{\partial \Psi}{\partial X}\frac{\partial \theta}{\partial Y} = \frac{1}{\mathrm{Re\,Pr}}\left(\frac{\partial^2 \theta}{\partial X^2} + \frac{\partial^2 \theta}{\partial Y^2}\right) \tag{11}$$

The quadratic interpolation function has been considered for the stream function, the vorticity function and the non-dimensional temperature.

$$\left.\begin{aligned} \Psi(X,Y) &= N_j^e \Psi_j^e \\ \Omega(X,Y) &= N_j^e \Omega_j^e \\ \theta(X,Y) &= N_j^e \theta_j^e \end{aligned}\right\} \tag{12}$$

where $i = 1,2,3,...,6$, N_i are the element interpolation functions.

The considered triangular element has three nodes. Therefore the interpolation functions are three noded triangular shape functions. All three nodes are associated with the stream function, the vorticity function and the non-dimensional temperature. To derive the finite element equations, the method of weighted residuals is applied to the Eqs. (9) – (11) and the Gauss's theorem is applied to generate the boundary integral terms associated with the surface tractions.

Continuity equation:

$$\frac{\partial^2\Psi}{\partial X\partial Y}-\frac{\partial^2\Psi}{\partial X\partial Y}=0$$

$$\Rightarrow \int_{\Lambda^e}\left(\frac{\partial^2\Psi}{\partial X\partial Y}-\frac{\partial^2\Psi}{\partial X\partial Y}\right)N_i d\Lambda^e=0$$

$$\Rightarrow \int_{\Lambda^e}\left[\frac{\partial}{\partial X}\left(\frac{\partial\Psi}{\partial Y}\right)-\frac{\partial}{\partial Y}\left(\frac{\partial\Psi}{\partial X}\right)\right]N_i d\Lambda^e=0$$

$$\Rightarrow \int_{\Lambda^e}\left(-\frac{\partial N_i^e}{\partial X}\frac{\partial N_j^e}{\partial Y}+\frac{\partial N_i^e}{\partial Y}\frac{\partial N_j^e}{\partial X}\right)\Psi_j^e d\Lambda^e+\int_{\Gamma^e}\left(\frac{\partial\overline{\Psi}}{\partial Y}-\frac{\partial\overline{\Psi}}{\partial X}\right)N_i^e d\Gamma^e=0$$

where Λ^e is the element area and Γ^e is the element boundary condition.
The elements of the local matrices are as follow:

$$A_{ij}^{11}=\int_{\Lambda^e}\left(-\frac{\partial N_i^e}{\partial X}\frac{\partial N_j^e}{\partial Y}+\frac{\partial N_i^e}{\partial Y}\frac{\partial N_j^e}{\partial X}\right)d\Lambda^e$$

$$A_{ij}^{12}=A_{ij}^{13}=0$$

$$f_{i_1}^e=-\int_{\Gamma^e}\left(\frac{\partial\overline{\Psi}}{\partial Y}-\frac{\partial\overline{\Psi}}{\partial X}\right)N_i^e d\Gamma^e$$

Momentum equation:

$$\left(\frac{\partial\Psi}{\partial Y}\frac{\partial\Omega}{\partial X}-\frac{\partial\Psi}{\partial X}\frac{\partial\Omega}{\partial Y}\right)-\frac{1}{Re}\left(\frac{\partial^2\Omega}{\partial X^2}+\frac{\partial^2\Omega}{\partial Y^2}\right)-Ri\left(\frac{\partial\theta}{\partial X}\right)=0$$

$$\Rightarrow \int_{\Lambda^e}\left[\left(\frac{\partial\Psi}{\partial Y}\frac{\partial\Omega}{\partial X}-\frac{\partial\Psi}{\partial X}\frac{\partial\Omega}{\partial Y}\right)-\frac{1}{Re}\left(\frac{\partial^2\Omega}{\partial X^2}+\frac{\partial^2\Omega}{\partial Y^2}\right)-Ri\left(\frac{\partial\theta}{\partial X}\right)\right]d\Lambda^e=0$$

$$\text{Term I}=\int_{\Lambda^e}\left(\sum_{j=1}^{3}\Psi_j^e\frac{\partial N_j^e}{\partial Y}\sum_{k=1}^{3}\Omega_k^e\frac{\partial N_k^e}{\partial X}-\sum_{j=1}^{3}\Psi_j^e\frac{\partial N_j^e}{\partial X}\sum_{k=1}^{3}\Omega_k^e\frac{\partial N_k^e}{\partial Y}\right)N_i^e d\Lambda^e$$

$$\text{Term II}=-\frac{1}{Re}\int_{\Lambda^e}\left(\frac{\partial^2\Omega}{\partial X^2}+\frac{\partial^2\Omega}{\partial Y^2}\right)N_i^e d\Lambda^e$$

$$=\frac{1}{Re}\int_{\Lambda^e}\left(\frac{\partial N_i^e}{\partial X}\frac{\partial N_j^e}{\partial X}+\frac{\partial N_i^e}{\partial Y}\frac{\partial N_j^e}{\partial Y}\right)\Omega_j^e d\Lambda^e-\frac{1}{Re}\int_{\Gamma^e}N_i^e\left(\frac{\partial\overline{\Omega}}{\partial X}+\frac{\partial\overline{\Omega}}{\partial Y}\right)d\Gamma^e$$

$$\text{TermIII}=-Ri\int_{\Lambda^e}\left(\frac{\partial\theta}{\partial X}\right)N_i^e d\Lambda^e$$

$$=-Ri\int_{\Lambda^e}N_i^e\left(\frac{\partial N_j^e}{\partial X}\right)\theta_j^e d\Lambda^e$$

Therefore, the elements of the local matrices are:

$$A_{ij}^{21}=0$$

$$A_{ij}^{22}=\frac{1}{Re}\int_{\Lambda^e}\left(\frac{\partial N_i^e}{\partial X}\frac{\partial N_j^e}{\partial X}+\frac{\partial N_i^e}{\partial Y}\frac{\partial N_j^e}{\partial Y}\right)d\Lambda^e$$

$$A_{ij}^{23} = -Ri\int_{\Lambda^e}\left(\frac{\partial N_j^e}{\partial X}\right)N_i^e d\Lambda^e$$

$$f_{i_2}^e = \int_{\Gamma^e} N_i^e\left(\frac{\partial\bar{\Omega}}{\partial X}+\frac{\partial\bar{\Omega}}{\partial Y}\right)d\Gamma^e - \int_{\Gamma^e}\left(\sum_{j=1}^{3}\Psi_j^e\frac{\partial N_j^e}{\partial Y}\sum_{k=1}^{3}\Omega_k^e\frac{\partial N_k^e}{\partial X}-\sum_{j=1}^{3}\Psi_j^e\frac{\partial N_j^e}{\partial X}\sum_{k=1}^{3}\Omega_k^e\frac{\partial N_k^e}{\partial Y}\right)N_i^e\,d\Lambda^e$$

Energy equation:

$$\left(\frac{\partial\Psi}{\partial Y}\frac{\partial\theta}{\partial X}-\frac{\partial\Psi}{\partial X}\frac{\partial\theta}{\partial Y}\right)-\frac{1}{Re\,Pr}\left(\frac{\partial^2\theta}{\partial X^2}+\frac{\partial^2\theta}{\partial Y^2}\right)=0$$

$$\Rightarrow\int_{\Lambda^e}\left\{\left(\frac{\partial\Psi}{\partial Y}\frac{\partial\theta}{\partial X}-\frac{\partial\Psi}{\partial X}\frac{\partial\theta}{\partial Y}\right)-\frac{1}{Re\,Pr}\left(\frac{\partial^2\theta}{\partial X^2}+\frac{\partial^2\theta}{\partial Y^2}\right)\right\}N_i d\Lambda^e=0$$

$$\Rightarrow\int_{\Lambda^e}\left(\sum_{j=1}^{3}\Psi_j^e\frac{\partial N_j^e}{\partial Y}\sum_{k=1}^{3}\theta_k^e\frac{\partial N_k^e}{\partial X}-\sum_{j=1}^{3}\Psi_j^e\frac{\partial N_j^e}{\partial X}\sum_{k=1}^{3}\theta_k^e\frac{\partial N_k^e}{\partial Y}\right)d\Lambda^e$$

$$+\int_{\Lambda^e}\left(\frac{\partial N_i^e}{\partial X}\frac{\partial N_j^e}{\partial X}+\frac{\partial N_i^e}{\partial Y}\frac{\partial N_j^e}{\partial Y}\right)\theta_j^e d\Lambda^e=\frac{1}{Re\,Pr}\int_{\Gamma^e}N_i^e\left(\frac{\partial\bar{\theta}}{\partial X}+\frac{\partial\bar{\theta}}{\partial Y}\right)d\Gamma^e$$

The elements of the local matrices are:

$$A_{ij}^{31}=A_{ij}^{32}=0;$$

$$A_{ij}^{33}=\int_{\Lambda^e}\left(\frac{\partial N_i^e}{\partial X}\frac{\partial N_j^e}{\partial X}+\frac{\partial N_i^e}{\partial Y}\frac{\partial N_j^e}{\partial Y}\right)d\Lambda^e;$$

$$f_{i_3}^e=\int_{\Gamma^e}N_i^e\left(\frac{\partial\bar{\theta}}{\partial X}+\frac{\partial\bar{\theta}}{\partial Y}\right)d\Gamma^e-\int_{\Lambda^e}\left(\sum_{j=1}^{3}\Psi_j^e\frac{\partial N_j^e}{\partial Y}\sum_{k=1}^{3}\theta_k^e\frac{\partial N_k^e}{\partial X}-\sum_{j=1}^{3}\Psi_j^e\frac{\partial N_j^e}{\partial X}\sum_{k=1}^{3}\theta_k^e\frac{\partial N_k^e}{\partial Y}\right)d\Lambda^e$$

$$A_{ij}^{31}=A_{ij}^{32}=0;$$

$$A_{ij}^{33}=\int_{\Lambda^e}\left(\frac{\partial N_i^e}{\partial X}\frac{\partial N_j^e}{\partial X}+\frac{\partial N_i^e}{\partial Y}\frac{\partial N_j^e}{\partial Y}\right)d\Lambda^e;$$

$$f_{i_3}^e=\frac{1}{Re\,Pr}\int_{\Gamma^e}N_i^e\left(\frac{\partial\bar{\theta}}{\partial X}+\frac{\partial\bar{\theta}}{\partial Y}\right)d\Gamma^e-\int_{\Lambda^e}\left(\sum_{j=1}^{3}\Psi_j^e\frac{\partial N_j^e}{\partial Y}\sum_{k=1}^{3}\theta_k^e\frac{\partial N_k^e}{\partial X}-\sum_{j=1}^{3}\Psi_j^e\frac{\partial N_j^e}{\partial X}\sum_{k=1}^{3}\theta_k^e\frac{\partial N_k^e}{\partial Y}\right)d\Lambda^e$$

$$K_{ij}^e=\begin{bmatrix}A_{ij}^{11} & A_{ij}^{12} & A_{ij}^{13}\\ A_{ij}^{21} & A_{ij}^{22} & A_{ij}^{23}\\ A_{ij}^{31} & A_{ij}^{32} & A_{ij}^{33}\end{bmatrix};\qquad a_i^e=\begin{bmatrix}\Psi_i^e\\ \Omega_i^e\\ \theta_i^e\end{bmatrix};\qquad f_i^e=\begin{bmatrix}f_{i_1}^e\\ f_{i_2}^e\\ f_{i_3}^e\end{bmatrix};$$

Then the local matrices are assembled in order to form the global matrices.

$$\sum_{i=1}^{n}\left[K_{ij}^e\right]\left[a_{ij}^e\right]=\left[f_i^e\right]$$

where n is the number of elements in the domain.

4. COMPUTATIONAL PROCEDURE

The numerical procedure used to solve the governing equations for the present work is based on the Galerkin weighted residual method of finite-element formulation. The application of this technique is well documented Reddy and Gartling (1994). The non-linear parametric solution method is chosen to solve the governing equations. This

approach will result in substantially fast convergence assurance. A non-uniform triangular mesh arrangement is implemented in the present investigation especially near the corrugated walls to capture the rapid changes in the dependent variables. To test and assess the grid independence of the present solution, several numerical runs are performed for higher Richardson numbers as shown in Table 1. These results reveals that a non-uniform spaced grid of approximately 60000 nodes for the solution domain is adequate to describe correctly the flow and heat and mass transfer processes inside the cavity. The present numerical approach was verified against the results published by Manca *et al.* (2003) for mixed convection heat transfer in open-ended enclosures with straight vertical walls for Richardson number $Ri = 0.1$, as shown in Table 2. It is seen in this comparison that both solutions are in good agreement.

Table 1: Comparison of the results for various grid dimensions ($Ri = 10$, C.F. = 1)

Nodes	20721	25102	42028	61983	76205	106417
Nu	2.866	2.611	2.733	2.744	2.744	2.744
θ_{max}	0.619	0.659	0.644	0.642	0.642	0.642

Table 2. Comparison of the results for validations at $Ri = 0.1$ and C.F. = 0 (Straight)

	Present	Manca *et al.* (2003)
Nu	1.670	1.674
θ_{max}	1.053	1.048

5. RESULTS AND DISCUSSIONS

In this investigation velocity vectors ($\vec{V} = \hat{i}U + \hat{j}V$), isotherms, vertical velocity and temperature distributions at the horizontal mid-plane and average Nusselt number distribution have been examined and discussed for corrugation frequency (C.F.) 0, 0.5, 1, 1.5, 2, 2.5 and 3, Richardson number, Ri from 0.1 to 10, and Reynolds number, Re of 100. The higher value of Richardson number corresponds to buoyancy dominated flow while the lower limit represents significant forced convective flow compared to natural convection flow.

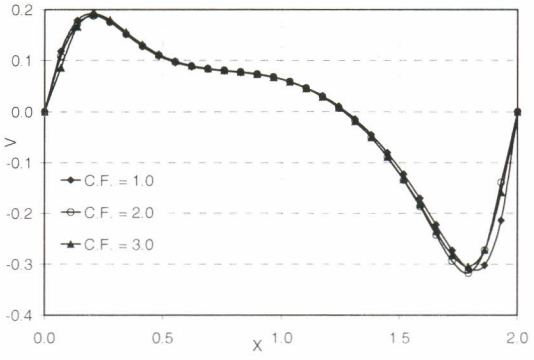

(a)

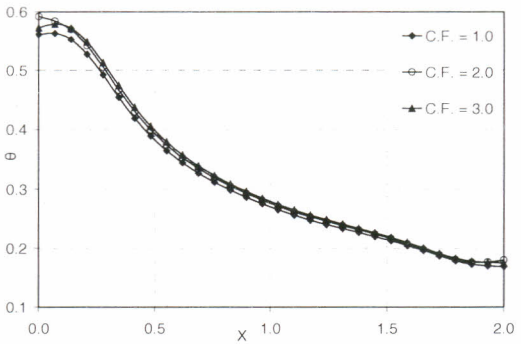

(b)

Fig. 2: Comparison of the velocity and temperature profiles at horizontal midsections of the enclosure for various corrugation frequencies (Ri = 1.0, Y = 0.5)

A. Effect of Corrugation Frequency

Figure 2 reveals the effect of corrugation on vertical velocity and temperature distribution at the horizontal mid-plane for different corrugation frequencies. In order to examine the buoyancy effect closely on the corrugated surface, the vertical velocity distribution along the mid-plane of the cavity is plotted instead of considering the horizontal velocity. It shows that the velocity profile remains almost constant with the change of corrugation frequency. However, the temperature gradient is lower near the corrugated wall whereas due to buoyancy effect, a large temperature variation sharply prevails away from the corrugated walls. This effect can be explained in details using Fig. 3 which shows the overall effect of corrugation frequency on the velocity vectors and isotherm inside the cavity. With the increases of corrugation frequency, both velocity and isotherm profile do not significantly change. But the symmetric behavior of the pattern of isotherms near the corrugated wall changes penetratingly which results in increase of the maximum temperature (θ_{max}) due to less circulation inside the cavity.

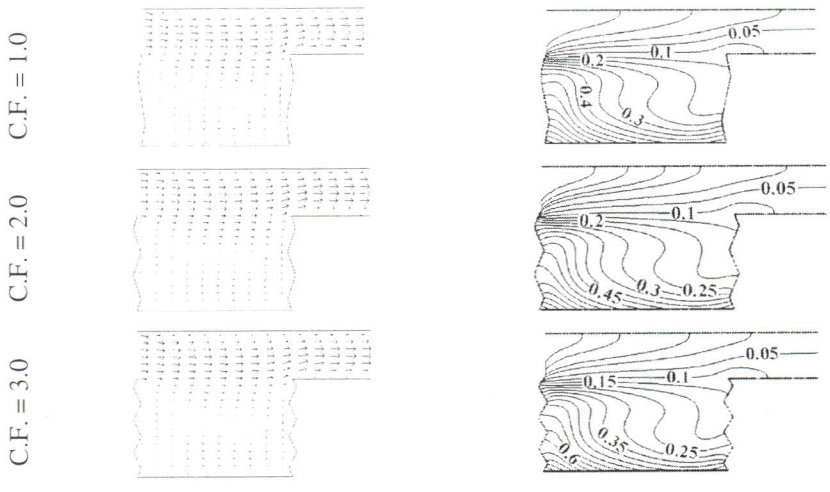

Fig. 3: Velocity vectors and isotherms at various corrugation frequencies for $Ri = 1.0$.

B. Effect of Richardson Number

The effect of Richardson number, *Ri* on the flow and temperature field at *Pr* = 0.7 is shown in Figs. 4 and 5. At lower values of *Ri* (mild buoyancy), the effect of shear is dominant relative to the buoyancy effect. A large primary eddy with large upstream forced flow and a nearly constant temperature core is observed with large temperature gradients in the near wall thermal boundary layer only. When *Ri* is changed from 0.1 to 1, the only effect of buoyancy is manifested through the change of location and size of the primary eddies. At *Ri* = 1, the location of primarily formed eddies shifted towards right and changes its strength to demonstrate the balance between shear and buoyancy effects. Though the velocity profile seems to be unaffected by the change of *Ri* to 1.0, a moderately decreasing trend of isotherm patterns can be found inside the cavity resulting in decrease of maximum temperature. When *Ri* is increased to 10, the large buoyancy effects are confined to thin thermal boundary layers only and a single primary vortex core with an approximately constant temperature is formed once again.

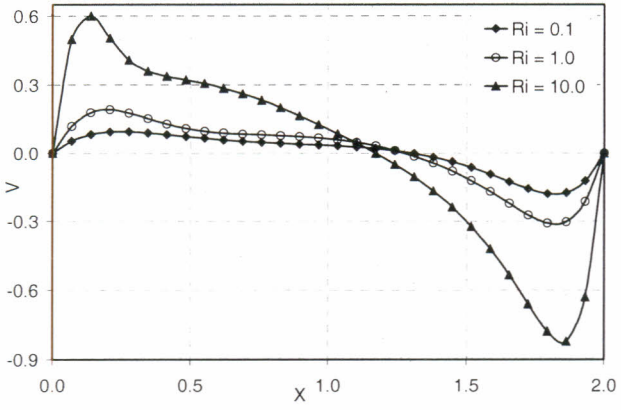

(a)

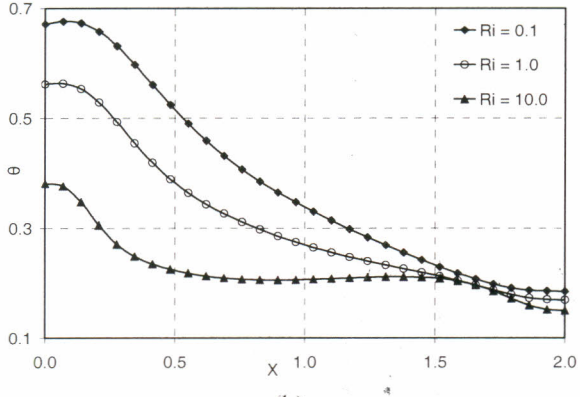

(b)

Fig. 4: Comparison of the velocity and temperature profiles at horizontal midsection of the enclosure for various Richardson numbers (C.F. = 1, *Y* = 0.5)

C. Nusselt Number Distribution

From Fig. 6, we can see that corrugation frequency plays a role on heat transfer for different values of Richardson number. The average heat transfer distribution shows that the heat transfer increases with the increase of Richardson number. But the corrugation frequency plays an interesting role on the convective heat transfer. From Fig. 6(a), we can observe an oscillatory behavior of maximum temperature for different corrugation frequency which concludes in Fig. 6(b) that maximum heat transfer occurs only in the case of corrugation frequency of 0.5.

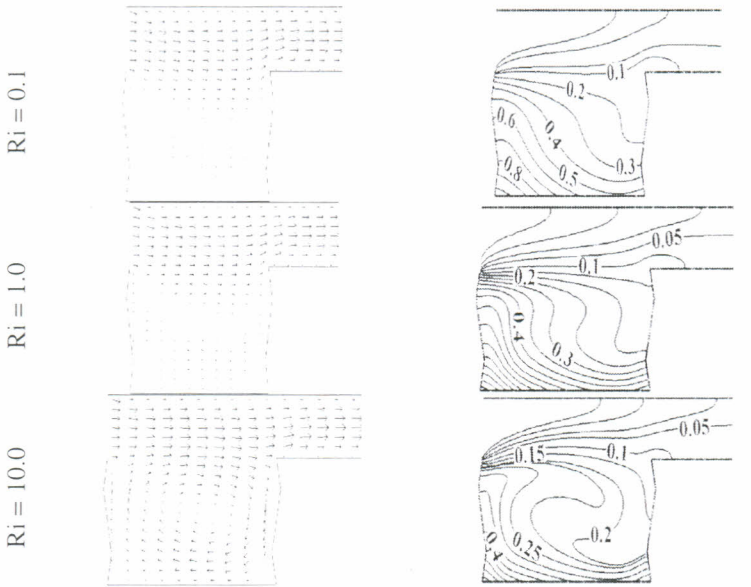

Fig. 5: Velocity vectors and isotherms at various Richardson numbers for C.F. = 1.0.

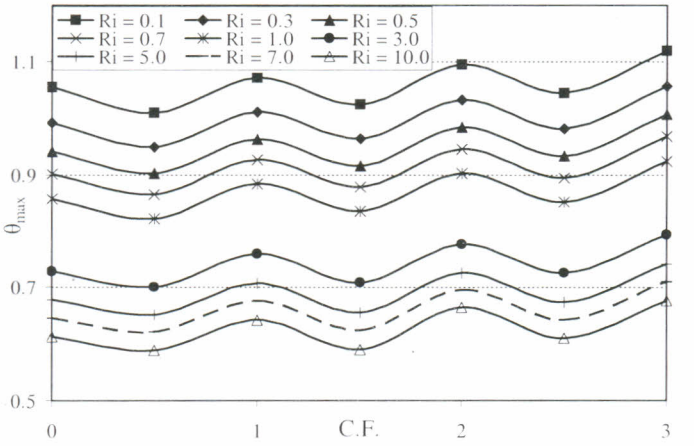

(a)

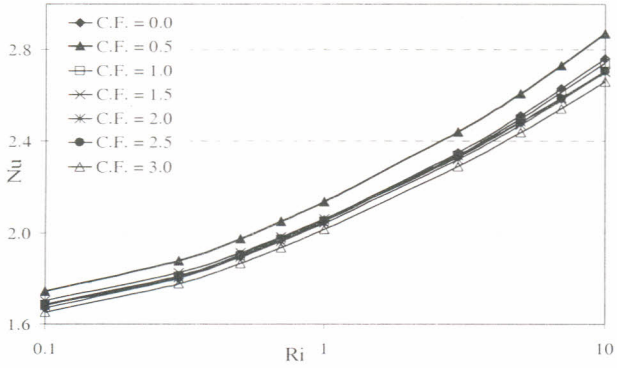

(b)

Fig. 6: Comparison of (a) the maximum temperature and (b) average Nus-selt number for various Ri and corrugation frequencies (Re=100, Pr = 0.7).

D. Heat Transfer Correlation

The average Nusselt numbers shown in Fig. 6(b) are correlated in terms of the corrugation frequency (C.F.) and the Richardson number for a Reynolds number of 100. The correlation obtained of the form:

$$Nu = 2.11 Ri^{0.111} C.F.^{-0.03} \qquad (13)$$

based on the numerical results for $0.1 \leq Ri \leq 10$ and $0.5 \leq$ C.F. ≤ 3 and an overall correlation coefficient of 0.988.

5. CONCLUSION

In this paper, convection heat transfer due to both buoyancy induced flow and forced flow inside a corrugated open enclosure of laminar region is numerically investigated. The above analysis shows that the overall heat transfer decreases with the increase of corrugation frequency. Also the maximum heat transfer obtained for corrugation frequency 0.5. Effect of buoyancy parameter for mixed convection in a bottom heated corrugated cavity is also studied. This result shows that the heat transfer increases with the increases of *Ri* for any corrugation frequency. From the computed data for different flow and geometry investigated, a simple algebraic correlation has been established for the average Nusselt number as a function of operating parameters.

NOMENCLATURE

A	Aspect ratio of the enclosure
c_p	Specific heat
C.F.	Corrugated frequency
D	Half of the height of the enclosure
g	Gravitational acceleration
Gr	Grashof number
h	Local convective heat transfer coefficient
H	The height of the inflow and outflow openings
L	Length of the heat source

N_i	The element interpolation functions
Nu	Nusselt number
p	Dimensional pressure
P	Dimensionless pressure
Pr	Prandtl number
q	Heat flux at the source
Ri	Richardson number
Re	Reynolds number
T	Dimensional temperature
T_i	uniform temperature
u_i	uniform velocity
u	Dimensional velocity component in x-direction
U	Dimensionless velocity component in x-direction
U_0	Constant speed
v	Dimensional velocity component in y-direction
V	Dimensionless velocity component in y-direction
W	Height of the enclosure
x, y	Dimensional coordinates
X, Y	Non-dimensional coordinates
Greek Symbols	
k	Thermal conductivity of fluid
α	Thermal diffusivity
θ	Dimensionless temperature
ρ	Fluid density
β	Thermal expansion coefficient
υ	Kinematic viscosity
Ψ	Stream function
φ	Any dependent variables
Ω	Vorticity function
Λ	Element area
Γ	Element boundary

REFERENCES

Ali, M. and Husain, S. R., 1992. Natural convection heat transfer and flow characteristics in a square duct of vee-corrugated vertical walls, *Journal of Energy, Heat and Mass Transfer*, vol. 14, pp. 125-131.

Ali, M. and Husain, S. R., 1993. Effect of corrugation frequencies on natural convection heat transfer and flow characteristics in a square enclosure of vee-corrugated vertical walls, *Int. J. of Energy Research*, vol. 17, pp. 697-708.

Ali, M., Das, D. K., and Zakir Hossain, M., 2001. Natural convection heat transfer in air confined by two vertical walls of different corrugation, *Int. Conference on Mechanical Engineering*, pp. 103-108.

Adjlout, L, Imine, O, Azzi, A., and Belkadi, M., 2002. Laminar natural convection in an inclined cavity with a wavy wall, *Int. J. Heat and Mass Transfer*, vol. 45, pp. 2141-2152.

Chinnappa, J. V. C., 1970. Free convection in air between a 60° vee-corrugated plate, *Int. J. Heat Mass Transfer*, vol. 13, pp. 117-123.

Das, P. K. and Mahmud, S., 2003. Numerical investigation of natural convection inside a wavy enclosure, *Int. J. Therm. Sci.*, vol. 42, pp. 397-406.

Fabbri, G., 2000. Heat transfer optimization in corrugated wall channels, *Int. J. Heat Mass Transfer*, vol. 43, pp. 4299-4310.

Kumar, B. V. R., 2000. A study of free convection induced by a vertical wavy surface with heat flux in a porous enclosure, *Num. Heat Transfer: Part A*, vol. 37, pp. 493-510.

Khanafer, K. and Vafai, K., 2000. Buoyancy-driven flow and heat transfer in open-ended enclosures: elimination of the extended boundaries, *Int. J. Heat Mass Transfer*, vol. 43, pp. 4087-4100.

Khanafer, K., Vafai, K., and Lightstone, M., 2002. Mixed convection heat transfer in two-dimensional open-ended enclosures, *Int. J. Heat Mass Transfer*, vol. 45, pp. 5171-5190.

Manca, O, Nardini, S., Khanafer, K., and Vafai, K., 2003. Effect of heated wall position on mixed convection in a channel with an open cavity, *Numerical Heat Transfer, Part A*, vol. 43, pp. 259-282.

Oosthuizen, P. H. and Paul, J. T., 1985. Mixed convective heat transfer in a cavity, *ASME-HTD*, vol. 42, pp. 159-169.

Papanicolaou, E. and Jaluria, Y., 1990. Mixed convection from an isolated heat source in a rectangular enclosure, *Numerical Heat Transfer, Part A*, vol. 18, pp. 427-461.

Papanicolaou, E. and Jaluria, Y., 1993. Mixed convection from a localized heat source in a cavity with conducting walls: a numerical study, *Numerical Heat Transfer, Part A*, vol. 23, pp. 463-484.

Randall, R. K., 1979. Interferometric investigation of convection in slat-flat plate and vee-corrugated solar collectors, Solar Energy International Progress, pp. 447-460.

Reddy, J. N. and Gartling, D. K., 1994. The finite element method in heat transfer and fluid dynamics, *CRC Press, Inc. Boca Raton, Florida.*

Simoneau, J. P., Inard, C., and Allard, F., 1988. Numerical approach of interaction between an injection and laminar natural convection in a thermally driven cavity, *ASME-HTD*, vol. 99, pp. 45-51.